

# PARALLEL ALGORITHM FOR TRACK INITIATION FOR OPTICAL SPACE SURVEILLANCE

P. Schumacher<sup>(1)</sup>, M. Wilkins<sup>(2)</sup>, C. Roscoe<sup>(2)</sup>

<sup>(1)</sup> Air Force Research Laboratory, 535 Lipoa Parkway, Suite 200, Kihei, Hawaii 96753

<sup>(2)</sup> Applied Defense Solutions, Inc., 10440 Little Patuxent Parkway, Suite 600, Columbia, Maryland 21044

## ABSTRACT

We propose a type of admissible-region analysis for track initiation in multi-satellite problems when angles are the primary observable. For a specified rectangular partition in the space of orbital elements, we present explicit upper and lower bounds, and other constraints, for the values of range and range rate that will lead to initial orbit hypotheses (data association hypotheses) associated with that partition. These bounds allow us to generate candidate orbits in an embarrassingly parallel fashion because each element-space partition can be handled independently of the others. Measured or derived angle rates provide additional bounds on range and range rate, also permitting the same parallelization.

## 1 INTRODUCTION

We begin with the angles-only case, in which angle rate values are not available or are too inaccurate for reliable use. Assume that we have a pair of line-of-sight unit vectors  $\mathbf{u}_i$  and  $\mathbf{u}_j$ , measured at time  $t_i$  at station position  $\mathbf{R}_i$  and time  $t_j$  at station position  $\mathbf{R}_j$ , respectively. Assume without loss of generality that  $t_j > t_i$ . We want to test the hypothesis that these two observations are associated with the same space object. To this end, we attach a set of hypothetical range values,  $\{\rho_{i,m}, m = 1, 2, \dots\}$  and  $\{\rho_{j,n}, n = 1, 2, \dots\}$  respectively, to each of these measured unit vectors and then generate candidate orbits by solving Lambert's problem for each of the pair-wise combinations of hypothetical orbital position vectors  $\mathbf{r}_{i,m} = \mathbf{R}_i + \rho_{i,m} \mathbf{u}_i$  and  $\mathbf{r}_{j,n} = \mathbf{R}_j + \rho_{j,n} \mathbf{u}_j$ . In principle, we can consider all possible pairs of observations and solve the family of Lambert problems for each pair. Then each hypothetical orbit from the solution of Lambert's problem is a data association hypothesis that must be either confirmed or eliminated through comparisons with other observational data. Given enough range hypotheses for each observed line of sight, we are guaranteed to generate a viable candidate orbit for every object that has been observed at two or more distinct times. However, the Cartesian product of the set of range values for each observed line of sight with the sets of range values from every other line of sight implies a possibly prohibitive number of Lambert solutions to generate and check. The computational complexity for generating hypothetical orbits on this

approach is quadratic in the number of observed lines of sight and also quadratic in the number of range hypotheses that we attach to the observations.

How should we limit the number of range hypotheses to make the total number of candidate orbits manageable while also generating candidates that are likely to correspond to real orbits of interest? For the purposes of this discussion, let us seek to generate hypotheses for orbits that lie only in a bounded region of semimajor axis  $a$ , eccentricity  $e$ , inclination  $I$  and right ascension of the ascending node  $\Omega$ , namely, within a partition of the element space specified by the intervals  $[a_{\text{MIN}}, a_{\text{MAX}}]$ ,  $[e_{\text{MIN}}, e_{\text{MAX}}]$ ,  $[I_{\text{MIN}}, I_{\text{MAX}}]$  and  $[\Omega_{\text{MIN}}, \Omega_{\text{MAX}}]$ . Then, to the extent that we can restrict the generation of hypothetical orbits to a specified partition of the space of orbital elements, we have parallelized the task of building a catalog of objects detected within that partition. The reason is that each partition can be handled independently. In the approach outlined here, all the observations would have to be considered for each partition of the space of orbit elements. However, by constructing upper and lower bounds on range for each measured line of sight for each partition of the element space, we limit the number of range hypotheses that have to be considered for each partition. This approach allows us to consider a manageable number of range hypotheses for each partition, simply by making the partitions small enough and using more processors to cover the whole element space.

We seek explicit bounds on range and possibly range rate that can be applied for each individual angle-based observation, or at most to pairs of angle-based observations. Even with the further restriction that hypothetical orbits be elliptical and Keplerian (which we accept) and even allowing the possibility that the observation may include angle rate values, it may not be obvious that efficient bounds having these properties can be obtained. Exact bounds would have to be based on some admissible-region analysis of the type developed by Milani [1], Tommei [2], Maruskin [3], Fujimoto [4] and others [5,6]. For example, denoting the gravitational parameter by  $\mu$ , we write the first integrals of Keplerian motion as

$$\text{energy: } E = (\dot{\mathbf{r}} \cdot \dot{\mathbf{r}})/2 - \mu/\|\mathbf{r}\| \quad (1)$$

$$\text{angular momentum: } \mathbf{h} = \mathbf{r} \times \dot{\mathbf{r}} \quad (2)$$

$$\text{Laplace vector: } \mu \mathbf{e} = \dot{\mathbf{r}} \times (\mathbf{r} \times \dot{\mathbf{r}}) - \mu \mathbf{r}/\|\mathbf{r}\| \quad (3)$$

Given the vector triangle relation  $\mathbf{r} = \mathbf{R} + \rho\mathbf{u}$  and its time derivative for each observation, we can define admissible regions in the  $(\rho, \dot{\rho})$  plane for each partition in the space of elements by means of inequalities such as

$$-\mu/(2a_{\text{MIN}}) \leq E \leq -\mu/(2a_{\text{MAX}}) \quad (4)$$

$$\cos I_{\text{MAX}} \leq (\mathbf{h}/\|\mathbf{h}\|) \cdot \mathbf{k} \leq \cos I_{\text{MIN}} \quad (5)$$

$$e_{\text{MIN}} \leq \|\mathbf{e}\| \leq e_{\text{MAX}} \quad (6)$$

Here  $\mathbf{k}$  is the north polar unit vector in the Earth-centered inertial frame. For each observation, the values of range and range rate that satisfy these inequalities will result in orbits that lie only within the given partition of the space of elements. DeMars and Jah [7] have shown what the admissible regions look like for partitions of semimajor axis and eccentricity by a numerical treatment of inequalities equivalent to (4)-(6). Maruskin, et al. [3], have shown how the admissible regions evolve in time and how the overlap of the admissible regions for different observations can help solve the data association problem. Tommei [5] and Farnocchia [6] have also addressed the data association problem in terms of admissible regions. However, even though Eqs. (1)-(6) can be reduced to polynomial forms in range and range rate, each relation is coupled in both variables and the polynomial degree is high, preventing us from obtaining explicit expressions for range and range rate in terms of the given data. Moreover, the usual admissible-region analysis leads nowhere if angle rates are not available. For example, the track-initiation method of DeMars, et al. [8,9], involving multiple hypotheses on range and range rate, requires both angle and angle rate values.

Our emphasis on generating candidate orbits with a Lambert-based approach in the angles-only case may require some explanation. Certainly, the bounds on range that we present here could be used in a variety of ways with other angles-based initial orbit determination methods. All the traditional methods of angles-only orbit determination, plus the modern methods of Gooding [10], Mortari and Karimi [11], and others, rely on solving for the range by either a root-finding method or an optimization method. Such algorithms can always be made to work more reliably when rigorous upper and lower bounds on the unknown quantity are available. However, one encounters at least three difficulties in trying to apply direct angles-only methods to a large, multiple-target catalog-building scenario.

First, although the range bounds presented here allow one to accept or reject candidate solutions based on range, for methods like Gooding's the range estimation is tantamount to the complete solution. Therefore, with a direct angles-only method one still has to compute the complete orbit solution in terms of the observations in order to find out if the range estimate satisfies the bounds. In our proposed Lambert-based approach, the

range bounds allow us to avoid most of the potential computation for the candidate orbits.

Second, the direct angles-only methods do not scale to large problems as well as a Lambert-based method does. Given  $N$  observations of line of sight, the computational load of Lambert-based methods is proportional to  $N^2$ , because two observations per data association hypothesis are needed. The "constant" of proportionality is itself quadratic in the number of range hypotheses that must be considered for each line of sight. However, as noted above, the latter number can be driven down to manageable size in each partition of the element space by making the partitions small. With traditional methods of angles-only initial orbit determination, one faces a computational load that is proportional to at least  $N^3$ , because at least 3 observations must be associated together to compute the range and hence the candidate orbit. The methods developed by Mortari and Karimi [11] are more robust than traditional methods, but these also require at least 3 observations per association hypothesis. In fact, the approach of Mortari and Karimi works better with more observations per association hypothesis, but then one faces a computational load that scales like  $N^4$ ,  $N^5$ , or even higher.

Third, a Lambert-based method, ideally implemented, will produce a candidate orbit for every object that has been observed at least twice. In comparison, a direct angles-based method, such as Gooding's, will produce candidate orbits only for those real objects that have been observed at least 3 times. An  $N^4$  method will produce candidate orbits only for those real objects that have been observed at least 4 times, and so on. Hence, the Lambert-based method may do a more complete job of generating viable candidate orbits from real datasets, while scaling more favorably than the direct angles-based methods for large numbers of observations.

In the present analysis, we take a geometric and kinematic approach that leads to explicit upper and lower bounds on the possible values of range for each observation, given only angle data at discrete times. In fact, we describe several inequalities that must be satisfied simultaneously, and we can take the most restrictive superposition of the different bounds as our working result. In case angle rates are available, we can obtain explicit upper and lower bounds on range rate, as well as additional bounds on range. It may happen that, for a given observation, there are no values of the range or range rate that lead to orbits within the given element-space partition, so that the observation can be eliminated from further consideration. We describe explicit conditions for the existence of possible values of range and range rate, in terms of the observation itself.

## 2 BOUNDS ON RANGE IMPLIED BY ANGLES

Here we describe bounds on range that must hold for each observed line of sight. Assuming that all orbits of interest are elliptical, require that the orbital radii lie between the maximum specified apogee and the minimum specified perigee:

$$[a_{\text{MIN}}(1 - e_{\text{MAX}})]^2 \leq \|\mathbf{r}\|^2 \leq [a_{\text{MAX}}(1 + e_{\text{MAX}})]^2 \quad (7)$$

The values of range that correspond to these limits on orbital radius can be found explicitly by inserting the vector triangle relationship  $\mathbf{r} = \mathbf{R} + \rho\mathbf{u}$ . Considering the perigee and apogee cases separately, we arrive at a set of quadratic inequalities that restrict the possible values of range to finite intervals. It is easy to isolate the range in these inequalities to produce explicit expressions for the allowable intervals. The requirement that range be non-negative further reduces these intervals. The requirement that range be real-valued identifies those observations for which no range consistent with the element partition is possible. If no range is possible, then we can eliminate the observation from further consideration and form no hypotheses with it. For each measured line of sight that is not eliminated in this manner for the element partition of interest, the set intersection of the intervals defined by the range inequalities becomes the hypothesis set from which we sample values of the range.

## 3 RESTRICTIONS IMPLIED BY THE SET OF ORBITAL PLANES

The above conditions are bounds on the possible values of range, which can be computed for each single observation. The fact that only single observations are involved is what allows us to find explicit bounds for each of the ranges before we form any range hypotheses. However, additional restrictions on the allowable values of range can be deduced from relations that involve both of the ranges presented for a solution to Lambert's problem. Although the nonlinearities in these relations prevent us from getting explicit inequalities, nevertheless we can formulate additional conditions that  $\rho_1$  and  $\rho_2$  must satisfy. Checking these extra conditions for each range pair may keep us from having to produce some unnecessary and relatively expensive Lambert solutions.

Using the vector triangle relation  $\mathbf{r} = \mathbf{R} + \rho\mathbf{u}$  for each of the two lines of sight, compute the unit vector  $\mathbf{n}$  normal to the candidate orbital plane:

$$\mathbf{n} = s(\mathbf{r}_1 \times \mathbf{r}_2) / \|\mathbf{r}_1 \times \mathbf{r}_2\| \quad (8)$$

Here the quantity  $s$  is a signum function:  $s = +1$  for "short-way" trajectories and  $s = -1$  for "long-way" trajectories. In general, we do not know *a priori* the sign

for  $s$  and both cases will need to be considered. With the sign chosen, the inclination is given unambiguously by

$$\cos I = \mathbf{n} \cdot \mathbf{k} \quad (9)$$

Hence we require that

$$\cos I_{\text{MAX}} \leq \mathbf{n} \cdot \mathbf{k} \leq \cos I_{\text{MIN}} \quad (10)$$

In the case of low-inclination intervals, it may be better to work in terms of sine inclination:

$$\sin I_{\text{MIN}} \leq \sqrt{1 - (\mathbf{n} \cdot \mathbf{k})^2} \leq \sin I_{\text{MAX}} \quad (11)$$

In a similar way, we use the unit nodal vector to obtain conditions that the range pair must satisfy if the candidate orbit is to lie within a specified interval of right ascension of the ascending node,  $[\Omega_{\text{MIN}}, \Omega_{\text{MAX}}]$ . In the Earth-centered inertial frame, we have

$$(\mathbf{k} \times \mathbf{n}) / \|\mathbf{k} \times \mathbf{n}\| = (\cos \Omega, \sin \Omega, 0)^T \quad (12)$$

so that, following standard logic for quadrant resolution, we require

$$\Omega_{\text{MIN}} \leq \tan^{-1}(\sin \Omega / \cos \Omega) \leq \Omega_{\text{MAX}} \quad (13)$$

Of course, for important special cases like near-GEO orbits, it may be preferable to define element partitions in terms of nonsingular elements such as  $p \triangleq \sin(I/2) \cos \Omega$  and  $q \triangleq \sin(I/2) \sin \Omega$ . No special difficulty attaches to working in terms of these or any other elements related to the orbit plane.

## 4 RESTRICTIONS IMPLIED BY LAMBERT'S THEOREM

We can also use three special solutions of Lambert's problem to restrict the ranges. The eccentricity of the orbit of least possible eccentricity that goes through a given pair of position vectors can be computed solely in terms of those position vectors. Call it  $e_0$ :

$$0 \leq e_0 = |(\|\mathbf{r}_1\| - \|\mathbf{r}_2\|) / \|\mathbf{r}_2 - \mathbf{r}_1\| \leq 1 \quad (14)$$

Likewise, the semimajor axis of the orbit of least possible semimajor axis that goes through the pair of positions can be computed solely in terms of the position vectors. Call it  $a_0$ :

$$4a_0 = \|\mathbf{r}_1\| + \|\mathbf{r}_2\| + \|\mathbf{r}_2 - \mathbf{r}_1\| \quad (15)$$

If  $a_0 > a_{\text{MAX}}$  or  $e_0 > e_{\text{MAX}}$ , then reject the range hypothesis pair without solving Lambert's problem, because the geometry is guaranteed to produce a larger semimajor axis or eccentricity than we have specified.

Next, Euler's Theorem, a special case of Lambert's Theorem, expresses the time of flight  $\Delta t_p$  between given position vectors on a parabolic (zero-energy) orbit:

$$\Delta t_p = \frac{4}{3} \sqrt{a_0^3/\mu} (1 - s \lambda^3) \quad (16)$$

Here again the quantity  $s$  is a signum function:  $s = +1$  for "short-way" trajectories and  $s = -1$  for "long-way" trajectories. The parameter  $\lambda$  is defined in terms of the position vectors:

$$0 \leq \lambda^2 = \frac{\|\mathbf{r}_1\| + \|\mathbf{r}_2\| - \|\mathbf{r}_2 - \mathbf{r}_1\|}{\|\mathbf{r}_1\| + \|\mathbf{r}_2\| + \|\mathbf{r}_2 - \mathbf{r}_1\|} \leq 1 \quad (17)$$

Because, for given position vectors, the time of flight in Lambert's problem is a monotonic decreasing function of the orbital energy, elliptic (negative-energy) orbits will always have a time of flight longer than the parabolic time, and hyperbolic (positive-energy) orbits will always have a time of flight shorter than the parabolic time. In our case, we can require that our observation pairs and range hypotheses always produce elliptic orbits:

$$t_2 - t_1 > \Delta t_p \quad (18)$$

Finally, the solution of Lambert's problem for elliptic orbits requires us to specify the number of complete orbital revolutions,  $N_{\text{REV}}$ , between the initial and final times. We cannot have an arbitrarily large number of revolutions in the given time of flight because the period of the orbit of minimum possible period  $T_0$  is fixed by the geometry of the problem:

$$T_0 = 2\pi \sqrt{a_0^3/\mu} \quad (19)$$

Accounting for the fact that some fraction of a revolution must remain after  $N_{\text{REV}}$  complete revolutions on the solution orbit, including possibly zero complete revolutions, the time of flight and number of revolutions must satisfy the inequality

$$t_2 - t_1 \geq N_{\text{REV}} T \quad (20)$$

where  $T$  is the actual period. Without solving Lambert's problem, we do not know  $T$ . However, the period is equal to or greater than  $T_0$ . Hence the time of flight must also satisfy the inequality

$$t_2 - t_1 \geq N_{\text{REV}} T_0 = 2\pi N_{\text{REV}} \sqrt{a_0^3/\mu} \quad (21)$$

Because of the unknown difference between  $T$  and  $T_0$ , it is possible that the number of complete revolutions allowed by Eq. (21) is larger than the true maximum

number of revolutions allowed in solutions of Lambert's problem.

If any range-pair hypothesis  $(\rho_1, \rho_2)$  does not satisfy Eqs. (8) and following, then that pair of values can be eliminated from further consideration without solving Lambert's problem. Note that it is the pair of range values that is eliminated; either range value by itself may still lead to an acceptable hypothesis in combination with some other range value.

## 5 BOUNDS ON RANGE AND RANGE RATE IMPLIED BY SIMULTANEOUS ANGLES AND ANGLE RATES

In case the observations include, or allow us to derive, angle rates, we can deduce additional bounds on the possible values of range. Like the bounds derived above from perigee and apogee distances, these extra bounds will apply to single observations, where we now understand an observation to consist of the values  $(\mathbf{R}, \dot{\mathbf{R}}, \mathbf{u}, \dot{\mathbf{u}})$  at a known time. Differentiating the vector triangle relation  $\mathbf{r} = \mathbf{R} + \rho \mathbf{u}$ , we get the orbital velocity:

$$\dot{\mathbf{r}} = \dot{\mathbf{R}} + \dot{\rho} \mathbf{u} + \rho \dot{\mathbf{u}} \quad (22)$$

The use of angle rate, when it is available, is especially important. If the observation includes simultaneous angles and angle rates, a complete orbit hypothesis can be formed for each observation without any iterative solutions, merely by choosing a value of range and a value of range rate. This is the approach outlined by DeMars et al. [8,9]. As in the angles-only case, the track-initiation problem is parallel with respect to element partitions. If we can provide bounds on range and range rate for each element partition, then we can reduce the number of orbit hypotheses needed for each partition simply by making the partitions smaller and using more processors to cover the whole element space. Bounds depending on angle rate will complement the range bounds already available from the angles-only case, and can be expected to further restrict the set of possible range hypotheses.

Most importantly, with accurate angle rate the track initiation job scales linearly with the number of observations rather than the square or cube of the number of observations. The problem also scales linearly in the number of range hypotheses and in the number of range rate hypotheses. One could hardly expect to do any better than this in solving a large track-initiation problem using optical data. Of course, nothing prevents us from using the improved bounds on range, and possibly range rate, to improve the efficiency of a Lambert-based approach. This choice may depend on whether the angle rates are accurate enough to represent the orbital state directly, or whether they should be used merely to provide extra bounds on the range.

We require the velocity magnitude to lie between the minimum possible apogee speed and the maximum possible perigee speed:

$$\frac{\mu}{a_{\text{MAX}}(1+e_{\text{MAX}})} \leq \|\dot{\mathbf{r}}\|^2 \leq \frac{\mu}{a_{\text{MIN}}(1-e_{\text{MAX}})} \quad (23)$$

We are looking for the region in the  $(\rho, \dot{\rho})$  plane implied by these inequalities. We define this region by the set-intersection of the intervals of range and range rate corresponding to each of the two inequalities. The quadratic form for velocity-squared, has no terms containing both range and range rate.

$$\|\dot{\mathbf{r}}\|^2 = \dot{\mathbf{R}} \cdot \dot{\mathbf{R}} + 2\dot{\rho}\dot{\mathbf{R}} \cdot \mathbf{u} + 2\rho\dot{\mathbf{R}} \cdot \dot{\mathbf{u}} + \dot{\rho}^2 + \rho^2 \dot{\mathbf{u}} \cdot \dot{\mathbf{u}} \quad (24)$$

Consequently, it is a simple matter to solve the inequalities for range in terms of range rate or for range rate in terms of range. Specifically, for each of the two cases, perigee and apogee, we can derive two equivalent sets of formulae.

First, solve the inequality in question for range rate in terms of range. The condition for having real values for range rate will involve a quadratic inequality in range. Solve this subsidiary inequality explicitly for range to find the interval of range over which real values for range rate occur. The requirement that range be non-negative further restricts the possible interval of range. Then, for each value of range in this interval, we obtain a corresponding pair of values of range rate. This pair defines the allowable interval of range rate at that value of range.

Second, solve the original inequality in question for range in terms of range rate. The condition for having real values for the range will involve a quadratic inequality in range rate. Solve this subsidiary inequality explicitly for range rate to find the interval of range rate over which real values for range occur. Then, for each value of range rate in this interval, we obtain a corresponding pair of values of range. This pair defines the interval of range at that value of range rate. The requirement that range be non-negative further restricts the allowable interval of range.

In either case, the level curves of the function (24) are ellipses in the  $(\rho, \dot{\rho})$  plane. The curves are approximately concentric with respect to a point defined by the observation. The set intersection of the intervals defined by the collection of inequalities for range and range rate lies between two ellipses and defines the region in the  $(\rho, \dot{\rho})$  plane from which we must sample hypothetical values of range and range rate.

## 6 ALGORITHM SUMMARY

For each range hypothesis  $\{\rho_{i,m}, m = 1, 2, 3, \dots\}$  associated with each line of sight vector  $\mathbf{u}_i$ , one will need

to test for all  $i$  and  $j \neq i$ , where  $t_j > t_i$ . Tab. 1 provides the summary algorithm.

Table 1. Acceptance algorithm for orbit hypotheses

Step	Acceptance Criteria for all $i, j \neq i, m$
1	$\mathbf{r}_i = \mathbf{R}_i + \rho_{i,m}\mathbf{u}_i$ $[a_{\text{MIN}}(1-e_{\text{MAX}})]^2 \leq \ \mathbf{r}_i\ ^2 \leq [a_{\text{MAX}}(1+e_{\text{MAX}})]^2$
2	$\mathbf{r}_j = \mathbf{R}_j + \rho_{j,m}\mathbf{u}_j, t_j > t_i$ $\mathbf{n} = s(\mathbf{r}_i \times \mathbf{r}_j) / \ \mathbf{r}_i \times \mathbf{r}_j\ , s = \pm 1$ $\cos I_{\text{MAX}} \leq \mathbf{n} \cdot \mathbf{k} \leq \cos I_{\text{MIN}}$
3	$(\mathbf{k} \times \mathbf{n}) / \ \mathbf{k} \times \mathbf{n}\  = (\cos \Omega, \sin \Omega, 0)^T$ $\Omega_{\text{MIN}} \leq \tan^{-1}(\sin \Omega / \cos \Omega) \leq \Omega_{\text{MAX}}$
4	$e_0 =  (\ \mathbf{r}_i\  - \ \mathbf{r}_j\ )  / \ \mathbf{r}_j - \mathbf{r}_i\ $ $4a_0 = \ \mathbf{r}_i\  + \ \mathbf{r}_j\  + \ \mathbf{r}_j - \mathbf{r}_i\ $ $a_0 < a_{\text{MAX}}$ and $e_0 < e_{\text{MAX}}$
5	$\lambda^2 = \frac{\ \mathbf{r}_i\  + \ \mathbf{r}_j\  - \ \mathbf{r}_j - \mathbf{r}_i\ }{\ \mathbf{r}_i\  + \ \mathbf{r}_j\  + \ \mathbf{r}_j - \mathbf{r}_i\ }$ $t_j - t_i > \frac{4}{3}\sqrt{a_0^3/\mu}(1-s\lambda^3), s = \pm 1$
6	$t_j - t_i \geq 2\pi N_{\text{REV}}\sqrt{a_0^3/\mu}$
7	$\dot{\mathbf{r}}_i = \dot{\mathbf{R}}_i + \dot{\rho}_{i,m}\mathbf{u}_i + \rho_{i,m}\dot{\mathbf{u}}_i$ $\frac{\mu}{a_{\text{MAX}}(1+e_{\text{MAX}})} \leq \ \dot{\mathbf{r}}_i\ ^2 \leq \frac{\mu}{a_{\text{MIN}}(1-e_{\text{MAX}})}$

## 7 NUMERICAL EXAMPLES

The results of the previous sections can be illustrated by a couple of simple examples. In this section we focus on the case of simultaneous observation of angles and angle rates since the use of both of these data types offers an opportunity for reduction in complexity of the problem compared to using angle data alone. In the following examples, we assume Keplerian motion with error-free measurements of angles and angle rates.

The first example assumes a station located at the origin. Therefore, the line-of-sight to the space object will be in the same direction as its position vector. Tab. 2 lists the relevant position, velocity and orbit quantities of the system. The element partitions used for semimajor axis and eccentricity are listed in Tab. 3.

Table 2. Orbital and Observational Data for Example 1

Quantity	Value
$\mathbf{R}, \dot{\mathbf{R}}$	[0, 0, 0] km, km/sec
$\mathbf{r}$	[2624, -10603, 5247] km
$\dot{\mathbf{r}}$	[3.673, -1.272, -4.408] km/sec
$\rho$	12118 km
$\dot{\rho}$	0 km/sec
$a$	12756 km
$e$	0.05

Table 3. Element Partition for Example 1

Element	Partition (min, max)
$a$	(11756, 13756) km
$e$	(0.03, 0.09)

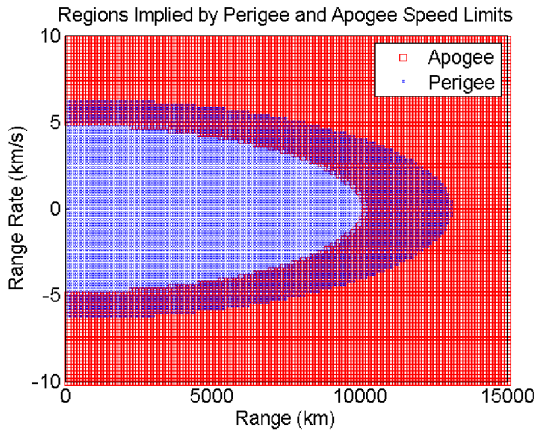


Figure 1. Overlapping range-range rate hypothesis regions for Example 1.

The maximum perigee velocity and minimum apogee velocity inequalities produce regions in the range-range rate plane which correspond to the selected partition of semimajor axis and eccentricity for the given angle and angle rate observation. For Example 1, these two regions are shown in Fig. 1. Note that the perigee condition is satisfied within an elliptical region whereas the apogee condition is satisfied outside a similar region. If a given observation were to form a pair of regions which had no overlap, then that observation would not lie within the selected element partition and could be eliminated from consideration.

The set intersection of these two regions forms the range-range rate hypothesis set for the given observation and is shown in Fig. 2.

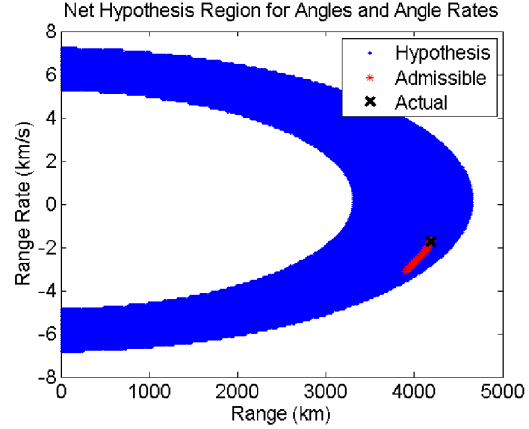


Figure 2. Range-range rate hypothesis set and admissible region for Example 1.

Note that ranges are restricted to positive values but range rate can be negative. The actual range and range rate for this observation are shown with the symbol “x” that lies within the hypothesis set as expected since the selected element partition contains the actual semimajor axis and eccentricity. Shown in red in Figure 2 is the exact admissible region for the given element partition. This region contains those range-range rate pairs which produce orbit solutions lying within the element partition. This region is typically smaller than the full hypothesis set. Part of the reason is that the latter set was derived without enforcing the  $e_{\text{MIN}}$  boundary of the partition, since  $e_{\text{MIN}}$  does not affect the range and range rate bounds offered in this paper. The admissible region shown in Fig. 3 does explicitly reflect the  $e_{\text{MIN}}$  constraint. If  $e_{\text{MIN}}$  is made large enough, the admissible region may break into disjoint sets, although the whole admissible region is always contained within our hypothesis set.

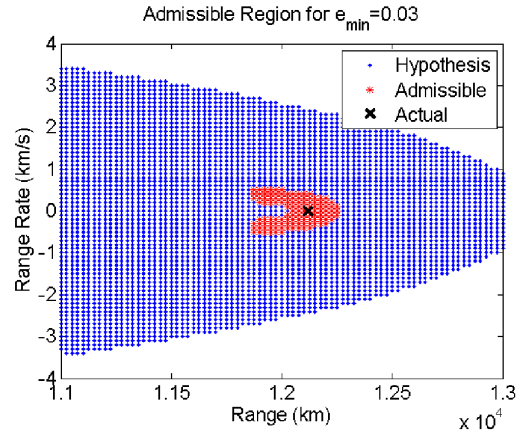


Figure 3. Admissible region with  $e_{\text{min}} = 0.03$  for Example 1.

Finally, Fig. 4 shows the same hypothesis set and admissible regions as in Fig. 2, along with the range

bounds implied by the minimum-perigee and maximum-apogee inequalities based on angle data only.

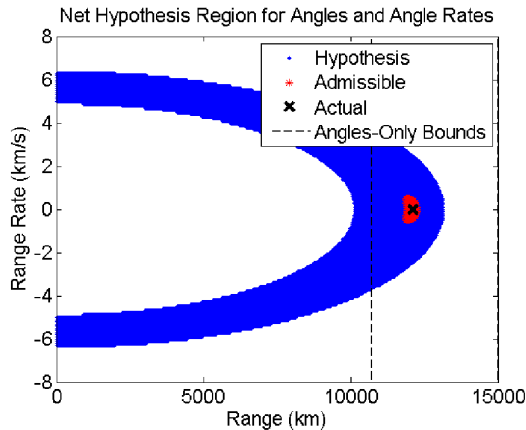


Figure 4. Range-range rate hypothesis set with angles-only range bounds for Example 1.

In this particular case, the combination of the angles-only range bounds with the range-range rate bounds derived from angle-angle rates produces a fairly small hypothesis set for the given observation.

The position, velocity, observation, and orbit quantities for the second example are listed in Tab. 4, and the element partition is listed in Tab. 5. Here the ground station is on the surface of the Earth and has a non-zero velocity.

Table 4. Orbital and Observational Data for Example 2

Quantity	Value
$\mathbf{R}$	[4092, 2690, 4076] km
$\dot{\mathbf{R}}$	[-0.196, 0.298, 0] km/sec
$\mathbf{r}$	[8102, 2576, 5271] km
$\dot{\mathbf{r}}$	[-2.683, 5.383, 2.786] km/sec
$\rho$	4185 km
$\dot{\rho}$	-1.724 km/sec
$a$	11149 km
$e$	0.145

Table 5. Element Partition for Example 2

Element	Partition (min, max)
$a$	(11049, 11249) km
$e$	(0, 0.1555)

The maximum perigee velocity and minimum apogee velocity hypothesis regions are shown in Fig. 5 and the net hypothesis set is shown in Fig. 6, along with the admissible region and actual range-range rate values. As before, the hypothesis set is shown along with the angle-implied range bounds in Fig. 7.

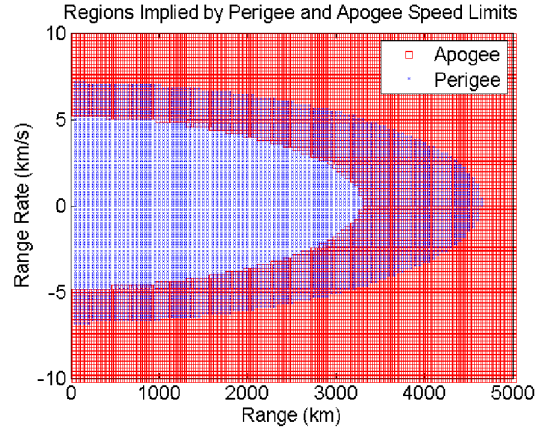


Figure 5. Overlapping range-range rate hypothesis regions for Example 2.

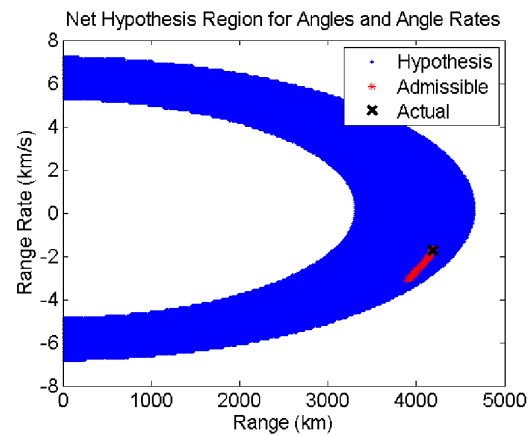


Figure 6. Range-range rate hypothesis set and admissible region for Example 2.

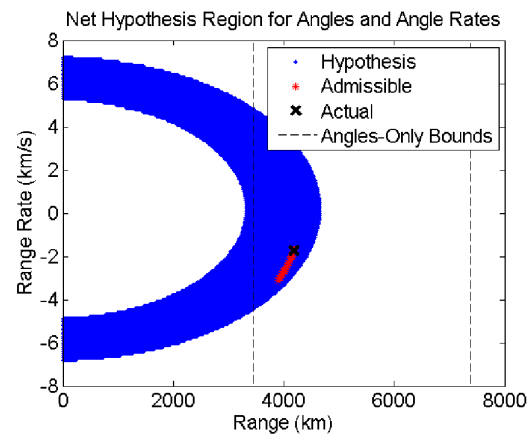


Figure 7. Range-range rate hypothesis region along with angles-only range bounds for Example 2.

## 8 SUMMARY AND CONCLUSION

Our results show that the possible values of range and range rate can be limited *a priori* for each line-of-sight

observation to finite intervals corresponding to a specified partition of the element space. The endpoints of the intervals are given explicitly in terms of the angle-based observations, station position and station velocity, and can be computed independently for each observation. In the angles-only case, additional conditions based on special solutions of Lambert's problem, which must be satisfied by range values for pairs of observations, can be used to further reduce the number of Lambert solutions needed for the initial orbit determinations. We also describe explicit conditions identifying when a given observation does not correspond to any possible orbit within the specified element-space partition. Such observations can be discarded before any data association hypotheses or orbit solutions are produced.

The range and range rate bounds described in this paper allow a convenient parallelization of the task of computing initial orbits in large space surveillance tracking scenarios, which is the phase of the tracking job that involves most of the computational complexity. Because the bounds are conservative to some extent and not exact, some values of range and range rate that lie within the bounds given here will lead to candidate orbits that lie outside the specified partition of the element space. This fact leads to some inefficiency in the parallelization of the initial orbit hypotheses over the whole element space. Essentially, Lambert solutions that lie outside the specified element partition must be discarded or moved to the correct partition, or else nearly duplicated candidate orbits would be generated and would therefore have to be identified and merged later in the tracking process. Each of these choices involves some "overhead" in the processing. Of course, the detection and merging of duplicate tracks must always be done in any multiple-hypothesis tracking job. However, the inefficiency of our range and range rate bounds necessarily increases the size of that task, unless we move or discard many Lambert solutions to prevent the duplication. The actual cost of this inefficiency in particular problems will depend on the observation sets, the element partitions of interest and the range / range-rate sampling strategy, and may need to be studied if the scenario is computationally stressing. On the other hand, all the orbits within an element-space partition correspond to values of range and range rate that lie within the bounds given here, so that no candidate orbits will be missed merely through this choice of bounds.

## 9 REFERENCES

1. Andrea Milani, Giovanni F. Gronchi, Mattia De'Michieli Vitturi and Zoran Knezevic (2004). Orbit Determination with Very Short Arcs: I. Admissible Regions. *Celestial Mechanics and Dynamical Astronomy* **90**, 59 – 87.
2. G. Tommei, A. Milani and A. Rossi (2007). Orbit determination of space debris: admissible regions. *Celestial Mechanics and Dynamical Astronomy* **97**, 289 – 304.
3. J.M. Maruskin, D.J. Scheeres and K.T. Alfriend (Jan.-Feb. 2009). Correlation of Optical Observations of Objects in Earth Orbit. *Journal of Guidance, Control and Dynamics* **32**(1), 194 – 209.
4. K. Fujimoto, J.M. Maruskin and D.J. Scheeres (2010). Circular and zero-inclination solutions for optical observations of Earth-orbiting objects. *Celestial Mechanics and Dynamical Astronomy* **106**, 157 – 182.
5. G. Tommei, A. Milani, D. Farnocchia and A. Rossi (30 Mar.-2 Apr. 2009). Correlation of Space debris Observations by the Virtual Debris Algorithm. *Proceeding of the Fifth European Conference on Space Debris*, European Space Operations Center, Darmstadt, Germany.
6. Davide Farnocchia, Giacomo Tommei, Andrea Milani and Alessandro Rossi (2010). Innovative methods of correlation and orbit determination for space debris. *Celestial Mechanics and Dynamical Astronomy* **107**, 169 – 185.
7. Kyle J. DeMars and Moriba K. Jah (29 Jan.-2 Feb. 2012). Initial Orbit Determination via Gaussian Mixture Approximation of the Admissible Region. AAS Paper 12-260, *Proceedings of the 22<sup>nd</sup> AAS/AIAA Space Flight Mechanics Conference*, , Charleston, South Carolina. *Advances in the Astronautical Sciences* **143**, Univelt Inc., San Diego, California.
8. Kyle J. DeMars, Moriba K. Jah and Paul W. Schumacher, Jr. (14-17 Feb. 2010). The Use of Angle and Angle Rate Data for Deep-Space Orbit Determination and Track Association. AAS Paper 10-153, *Proceedings of the 20<sup>th</sup> AAS/AIAA Space Flight Mechanics Conference*, San Diego, California. *Advances in the Astronautical Sciences* **136**, Univelt Inc., San Diego, California.
9. DeMars, K. J., Jah, M. K., and Schumacher, P. W. (Jul. 2012). Initial Orbit Determination using Short-Arc Angle and Angle Rate Data. *IEEE Transactions on Aerospace and Electronic Systems* **43**(3), 2628-2637.
10. R.H. Gooding (1997). A new procedure for the solution of the classical problem of minimal orbit determination from three lines of sight. *Celestial Mechanics and Dynamical Astronomy* **66**(4), 387 – 423.
11. Reza Raymond Karimi and Daniele Mortari (2011). Initial orbit determination using multiple observations. *Celestial Mechanics and Dynamical Astronomy* **109**(2), 167 – 180.